Experimental study of the quasifission, fusion-fission, and de-excitation of Cf compound nuclei

J. Khuyagbaatar,[1,2,*] D. J. Hinde,[3] I. P. Carter,[3] M. Dasgupta,[3] Ch. E. Düllmann,[1,2,4] M. Evers,[3] D. H. Luong,[3] R. du Rietz,[3] A. Wakhle,[3] E. Williams,[3] and A. Yakushev[2]

[1]*Helmholz Institute Mainz, 55099, Mainz, Germany*

[2]*GSI Helmholtzzentrum für Schwerionenforschung, 64291 Darmstadt, Germany*

[3]*Department of Nuclear Physics, RSPE, Australian National University, Canberra, Australian Capital Territory 2601, Australia*

[4]*Johannes Gutenberg-Universität Mainz, 55099 Mainz, Germany*

(Received 17 March 2015; revised manuscript received 14 April 2015; published 11 May 2015)

Background: The fusion-evaporation reaction at energies around the Coulomb barrier is presently the only way to produce the heaviest elements. However, formation of evaporation residues is strongly hindered due to the competing fusion-fission and quasifission processes. Presently, a full understanding of these processes and their relationships has not been reached.

Purpose: This work aims to use new fission measurements and existing evaporation residue and fission excitation function data for reactions forming Cf isotopes to investigate the dependence of the quasifission probability and characteristics on the identities of the two colliding nuclei in heavy element formation reactions.

Method: Using the Australian National University's 14UD electrostatic accelerator and CUBE detector array, fission fragments from the $^{12}C + ^{235}U$, $^{34}S + ^{208}Pb$, $^{36}S + ^{206}Pb$, $^{36}S + ^{208}Pb$, and $^{44}Ca + ^{198}Pt$ reactions were measured. Mass and angle distributions of fission fragments were extracted and compared to investigate the presence and characteristics of quasifission.

Results: Mass-angle-correlated fission fragments were observed for the $^{44}Ca + ^{198}Pt$ reaction; no correlation was observed in the other reactions measured. Flat-topped fission-fragment mass distributions were observed for $^{12}C + ^{235}U$ at compound-nucleus excitation energies from 28 to 52 MeV. Less pronounced flat-topped distributions were observed, with very similar shapes, for all three sulfur-induced reactions at excitation energies lower than 45 MeV.

Conclusions: A high probability of long-time-scale quasifission seems necessary to explain both the fission and evaporation residue data for the $^{34}S + ^{208}Pb$ and $^{36}S + ^{206}Pb$ reactions. Flat-topped mass distributions observed for ^{12}C- and $^{34,36}S$-induced reactions are suggested to originate both from late-chance fusion-fission at low excitation energies and the persistence of shell effects at the higher energies associated with quasifission.

DOI: 10.1103/PhysRevC.91.054608 PACS number(s): 25.70.Jj, 27.90.+b, 25.70.Gh

I. INTRODUCTION

The complete fusion of two colliding nuclei forming a compact excited compound nucleus (CN) is a topic of wide interest in nuclear physics. In particular, the de-excitation of this CN largely through the evaporation of neutrons is vital since it gives access to nuclei that do not exist in nature. To date, the heaviest elements (with proton numbers $Z = 104$–118) have been exclusively synthesized in such reactions, known as fusion-evaporation [1–4], with the heavy fusion products called evaporation residues (ERs).

A significant difficulty in producing the heaviest elements in fusion-evaporation reactions is their low cross sections, which generally decrease drastically with increases in the proton number of the CN. Thus, often multiday, weeks-long, and months-long experiments are needed for the observation of a single atom of a superheavy element [1–5]. Furthermore in fusion reactions, the excitation energy and the angular momentum introduced reduce the fission barrier height [6,7] relative to the already low ground-state fission barrier. Thus fission becomes the main de-excitation mode of the CN. Therefore, the formation of heavy evaporation residues is strongly suppressed relative to CN production.

ER formation is also suppressed by the process of quasifission (QF). This occurs when the two colliding nuclei initially forming a dinuclear system fail to reach equilibration in all degrees of freedom. Thus they may never form the compact CN required for the subsequent survival of ER. Quasifission competition can depend strongly on the identities and characteristics of the two colliding nuclei [8–19]. As a result, ER cross sections for different projectile and target combinations, even when leading to the formation of the *same* CN, can vary drastically [15,18]. Therefore, choosing a suitable projectile-target combination and optimum beam energy for a reaction are the most important factors for maximizing the yield of heavy nuclei.

The ER cross section following a fusion reaction leading to a CN at excitation energy E^* and angular momentum J can be written as

$$\sigma_{\rm ER}(E^*,J) = \sigma_{\rm cap}(E^*,J)P_{\rm CN}(E^*,J)W_{\rm CN}(E^*,J), \quad (1)$$

where $\sigma_{\rm cap}$ is the cross section characterizing the formation of the dinuclear system (capture), $P_{\rm CN}$ is the probability to form a compound nucleus with a compact shape, and $W_{\rm CN}$ is the survival probability of the CN against fission through particle evaporation. The first and last terms are characteristic of the reaction entrance channel and the de-excitation of the CN, respectively, which are independent processes and

*J.Khuyagbaatar@gsi.de

thus, in principle, may be investigated independently, both experimentally and theoretically. The probability P_{CN} reflects the quasifission probability P_{QF}, because the processes are complementary, in other words $P_{CN} + P_{QF} = 1$. Knowledge of P_{CN} allows estimation of the true fusion cross section ($\sigma_{cap} P_{CN}$). P_{CN} defines the intermediate step between capture and the de-excitation process leading to ER formation.

For decades, the choice of the reactions used for the production of the heaviest nuclei has been based on our understanding of the nuclear reaction mechanisms achieved from comparative studies of fission fragments from fusion-fission and quasifission [8–13]. It has been found that fission fragments originating from quasifission are often characterized by their broad mass distribution, mass and angle correlation, total kinetic energy, angular distributions, etc., which indicate a nonequilibrium origin and short sticking time of the decaying system compared to those originating from fusion-fission [8,9,12,13]. The presence of quasifission ($P_{CN} < 1$) has been predicted theoretically for reactions with projectile-target charge products $Z_p Z_t \geqslant 1600$ [8] and supported by the accumulated experimental data, where quasifission was mostly qualitatively assigned based on the abovementioned experimental observables connected with the short sticking time [9,12,13]. Estimation of the fractions of quasifission and fusion-fission from a single reaction is difficult due to overlaps in their experimental observables. Nevertheless, this has been attempted [16].

Various theoretical models for the prediction of fusion-evaporation cross sections have been developed [20–22]. Although they have been able to calculate experimental ER cross sections in satisfactory agreement with experiment, their predictive power, particularly of P_{CN} and W_{CN}, still remains to be improved [23].

Rigorous evidence for competition between quasifission and ER production can only be obtained through measurements of ER cross sections for reactions forming the *same* CN at the *same* E^* with different projectile-target combinations [24]. Thus neglecting angular momentum differences (reasonable for reactions forming highly fissile CN), survival probabilities W_{CN} should be the same, and the probability of quasifission can be directly probed by comparing σ_{ER}/σ_{cap} of different reactions. However, the relatively low production rates of ER, restricted numbers of possible projectile-target combinations, and experimental problems strongly limit such studies in reactions forming heavy nuclei. Nevertheless, a few experimental studies searching for the presence of quasifission have been performed through measurements of both ER and fission [24,25] for different reactions leading to the same CN. The results in Refs. [24,25] straightforwardly demonstrate the presence of quasifission in colliding systems with $Z_p Z_t$ much less than 1600, a finding which was corroborated in a recent analysis of mass and angle correlations of fission fragments [17]. This is consistent with experimental studies involving the measurements of ER and/or fission fragments from reactions with widely different $Z_p Z_t$, which had previously implied the presence of quasifission for $Z_p Z_t < 1600$ [10,11,16,18,26–35].

Among these, a most intriguing result has been found in a series of systematic studies of the $^{36}S + ^{206}Pb$ and $^{34}S + ^{208}Pb$ reactions (which of course share the *same* $Z_p Z_t$ value of

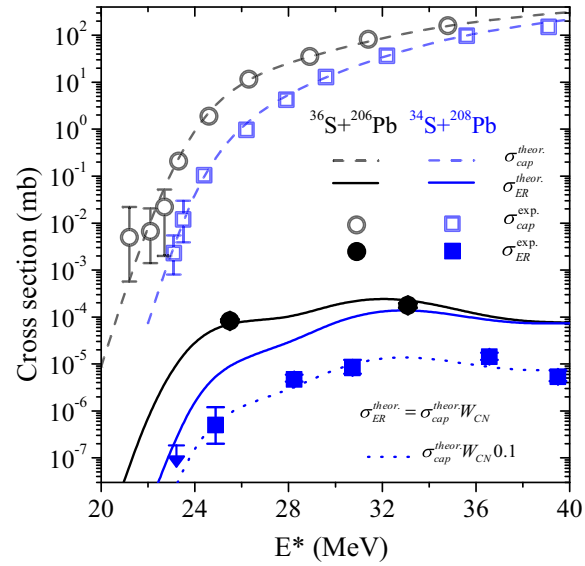

FIG. 1. (Color online) Experimental (symbols) capture and ER cross sections following neutron evaporation as a function of excitation energy for the reactions $^{36}S + ^{206}Pb$ and $^{34}S + ^{208}Pb$, both forming the same CN $^{242}Cf^*$ [25]. The downward arrow marks the upper cross-section limit. Theoretical ER cross sections indicated by solid lines were calculated assuming that no quasifission is present in either reaction ($P_{CN} = 1$). The dotted line represents calculations for $^{34}S + ^{208}Pb$ assuming that P_{CN} is 10 times smaller ($P_{CN} = 0.1$).

1312) leading to formation of the same CN $^{242}Cf^*$ [25]. The cross sections for ER following neutron evaporations (xn ER) [36] and capture cross sections [25], together with theoretical calculations [25], are shown in Fig. 1. The sum of only two- and three-neutron evaporation cross sections are representative of the total ER cross sections since other neutron and/or light particle evaporation channels are typically small in such reactions.

The calculations reproduce the measured capture cross sections for both reactions. Assuming no quasifission ($P_{CN} = 1$), the statistical model calculations of the fission survival probability W_{CN} are able to reproduce the measured xn ER cross sections for the $^{36}S + ^{206}Pb$ reaction. However, using the same parameters the experimental xn ER cross sections for the $^{34}S + ^{208}Pb$ reaction are overpredicted. They can be described by introducing a strong fusion hindrance relative to the $^{36}S + ^{206}Pb$ reaction (with an angular momentum averaged hindrance $P_{CN} = 0.1$), which must be associated with a greater quasifission probability for $^{34}S + ^{208}Pb$. Given that both reactions share the same $Z_p Z_t$ value, this observation gives new insight into the multidimensionality of the quasifission dynamics [16,37] and cannot be explained with existing models of heavy element formation.

Decades ago, measured fission angular distributions in the similar reaction $^{32}S + ^{208}Pb$ [10,11,38] suggested the presence of quasifission. However, this was never confirmed by ER measurements until the abovementioned $^{34}S + ^{208}Pb$ and $^{36}S + ^{206}Pb$ reactions were studied [36].

The present work aims to investigate the mass-angle and mass distributions of fission fragments for $^{34}S + ^{208}Pb$ and $^{36}S + ^{206}Pb$ to search for observable differences that might be

expected due to the different quasifission competition implied from the measurements of xn ER and capture cross sections.

II. EXPERIMENTAL SETUP

The experiment was carried out at the Heavy Ion Accelerator Facility at the Australian National University, Canberra. Heavy ion beams were accelerated using the 14UD electrostatic accelerator. In addition to $^{34}S + ^{208}Pb$ and $^{36}S + ^{206}Pb$ forming ^{242}Cf, two reference reactions ($^{44}Ca + ^{198}Pt$ and $^{12}C + ^{235}U$) were also measured. The $^{12}C + ^{235}U$ reaction leads to a different CN ($^{247}Cf^*$) than the other reactions studied. However, neither the $^{12}C + ^{230}U$ nor the $^{7}C + ^{235}U$ reaction (which lead to $^{242}Cf^*$) were experimentally accessible. quasifission is expected to be dominant in the $^{44}Ca + ^{198}Pt$ reaction and fusion-fission is expected to be dominant in the $^{12}C + ^{235}U$ reaction. Measurement for $^{36}S + ^{208}Pb$ was also carried out to help with interpretation in case large differences in fission characteristics were seen for the other two S + Pb reactions.

The ^{12}C, ^{34}S, and ^{36}S beams were used in a short pulsed mode with ≈ 1 ns full width at half maximum beam pulses separated by 107 ns. The ^{44}Ca beam (from natural calcium material) was used in the DC mode. Isotopically enriched ^{198}Pt, $^{206}PbCl_2$, ^{208}PbS, and $^{235}UO_2(NO_3)_2$ targets were used. Their thicknesses were approximately 145, 60, 180, and 14 $\mu g/cm^2$, respectively. Supporting thin carbon foils with typical thicknesses of 15–30 $\mu g/cm^2$ were used. The targets were placed at an angle of 60° relative to the beam axis, with the C-backing material downstream. Beam energies were chosen to form CN with similar excitation energies. Entrance channel quantities for all reactions are given in Table I.

Coincident fission fragments were measured using two position-sensitive multiwire proportional counters (MWPCs) with dimensions of 28×36 cm^2. They were mounted so that the centers of the MWPCs were located at laboratory scattering angles of 90° and 45° relative to the beam axis and separated by 180° in azimuthal angle. The distance from the center of each MWPC to the center of the target was 180 mm. Each MWPC covered scattering angle ranges of 55°–130° and 5°–80°. Two small Si surface-barrier detectors mounted symmetrically at a scattering angle of 30° on opposite sides of the beam axis were used to monitor the beam energy and flux.

For the pulsed beam experiments, the velocities of fission fragments were individually determined by measuring the time-of-flight for each fragment [17,41]. Only the difference in time-of-flight for each pair of coincident fission fragments was measured in the case of the DC beam [32]; this quantity was then used to calculate fragment velocities [17]. The measured positions and velocities of the fission fragments were then used to reconstruct the center-of-mass angle ($\theta_{c.m.}$) and mass ratio $M_R = m_1/(m_1 + m_2)$, where m_1 and m_2 are the two fragment masses at scission. A detailed description of the experimental setup and data analysis can be found in Refs. [17,31,32].

It is important to note that for $^{12}C + ^{235}U$, only fission events originating from fusion (forming the $^{247}Cf^*$ CN) were selected. The small fraction of fission events originating from fission of targetlike nuclei [28,41] was removed from the data by requiring full momentum transfer conditions for the measured fissionlike events [28,41].

TABLE I. Reaction Q values [39], charge products of the projectile and target (Z_pZ_t), excitation energies at the Bass fusion barrier (E_B^*) [40], and entrance channel mass asymmetries $\alpha = (A_t - A_p)/(A_p + A_t)$ are given.

Reaction	CN	Q (MeV)	E_B^* (MeV)	Z_pZ_t	α
$^{12}C + ^{235}U$	$^{247}Cf^*$	−25.2	39.5	552	0.90
$^{34}S + ^{208}Pb$	$^{242}Cf^*$	−111.0	35.0	1312	0.72
$^{36}S + ^{206}Pb$	$^{242}Cf^*$	−113.8	31.3	1312	0.70
$^{36}S + ^{208}Pb$	$^{244}Cf^*$	−113.9	30.9	1312	0.70
$^{44}Ca + ^{198}Pt$	$^{242}Cf^*$	−131.2	39.9	1560	0.64

III. EXPERIMENTAL RESULTS

A selection of the experimental data are presented in Fig. 2 as mass-angle distributions (MADs), where mass ratio M_R is plotted as a function of the center-of-mass angle $\theta_{c.m.}$ for reactions $^{12}C + ^{235}U$, $^{36}S + ^{206}Pb$, $^{34}S + ^{208}Pb$, and $^{44}Ca + ^{198}Pt$. MADs for the $^{36}S + ^{208}Pb$ reaction were similar to those

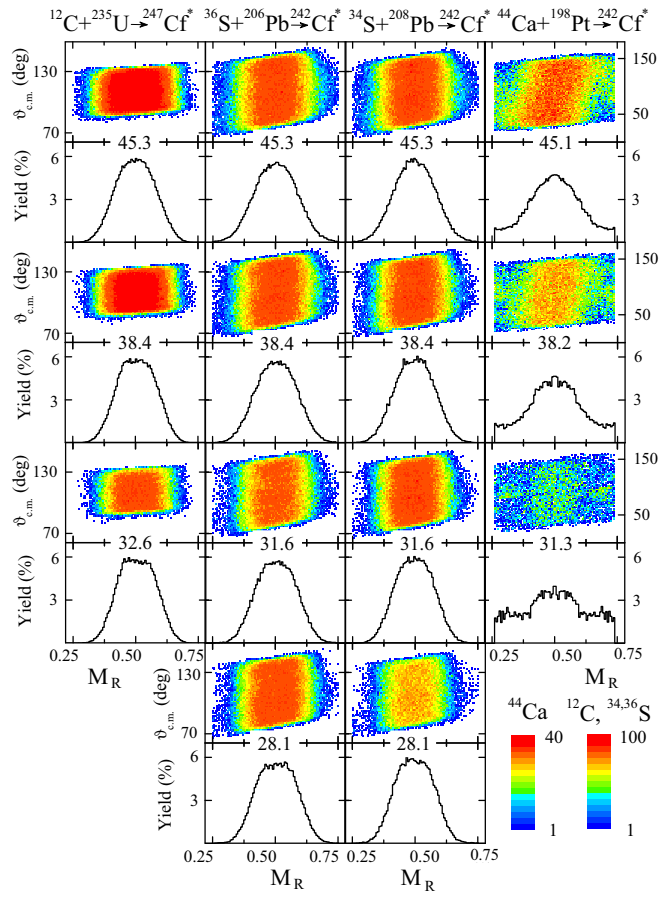

FIG. 2. (Color online) Measured mass and angle distributions of fission fragments from the reactions $^{12}C + ^{235}U$, $^{36}S + ^{206}Pb$, $^{34}S + ^{208}Pb$, and $^{44}Ca + ^{198}Pt$ are shown in the M_R and $\theta_{c.m.}$ plane. Below each MAD plot the projection of the MAD onto the M_R axis is shown (see text). Excitation energies of the corresponding CN (^{242}Cf and ^{247}Cf) are given.

for $^{36}S + ^{206}Pb$ and $^{34}S + ^{208}Pb$, and hence are not shown. MADs of fission fragments for ^{44}Ca are mirrored about $\theta_{c.m.} = 90^\circ$ and $M_R = 0.5$ [17], where mirroring highlights the mass-angle correlation trend. Fission fragments with mass ratios ranging from $M_R = 0.25$ (0.26 for ^{44}Ca) to 0.75 (0.74) were selected to exclude events from elastic and inelastic scattering.

In Fig. 2, projections onto the M_R axis are also shown for fission events within the angular range $90^\circ < \theta_{c.m.} < 132^\circ$ for the $^{12}C + ^{235}U$ reaction, and $88^\circ < \theta_{c.m.} < 138^\circ$ for the S-induced reactions, to exclude artificial asymmetry due to the angular acceptance of the detectors. In the M_R spectra for ^{44}Ca, shoulders at the extreme M_R values (most noticeable at the lower energies) are due to elastic and/or inelastic scattering, which were not clearly separated in data using the DC beam.

A. Mass-angle correlation

1. *Reference reactions*

The mass-angle distributions of fission fragments from the reaction $^{44}Ca + ^{198}Pt$ show a noticeable correlation between the mass ratio and the center-of-mass angle (hereafter, mass and angle) at all measured energies. This originates from the reseparation of the dinuclear system typically before completing one full rotation during evolution towards mass symmetry [9,12,13,31,32,42]. This evidence is the strongest indication of the dominance of quasifission, because a mass-angle correlation reflects directly the dynamical evolution of two captured nuclei that fail to fuse. A characteristic median time scale of $\leqslant 10^{-20}$ s has been found [42] to describe such experimental MADs, which agrees well with results obtained in Refs. [9,12,13] and reasonably well with the neutron-clock method [43]. $^{44}Ca + ^{198}Pt$ is an example of a typical reaction where quasifission is fast. The high Z_pZ_t (1560) results in strong Coulomb repulsion and together with the effect of angular momentum causes rapid breaking of the dinuclear system. Recently, it has been shown that the Z_pZ_t threshold for the appearance of fast quasifission resulting in such MAD can be lower than 1600, dependent on the fissility of the CN [17].

For the second reference reaction, $^{12}C + ^{235}U$, no correlation between the mass and angle was observed. This indicates the absence of fast quasifission, consistent with fission originating from a system that has made more than one full rotation. Because of the low Z_pZ_t of only 552, it would be expected (at least at above-barrier energies [28]) that fission fragments from the $^{12}C + ^{235}U$ reaction should overwhelmingly originate from fusion-fission.

2. S + Pb *reactions*

MADs of the $^{34}S + ^{208}Pb$ and $^{36}S + ^{206}Pb$ reactions, and also of the $^{36}S + ^{208}Pb$ reaction, show no mass-angle correlations. MADs from the first two reactions can be directly compared to those for the $^{44}Ca + ^{198}Pt$ reaction, because all lead to the same composite nucleus at the same excitation energies (see Fig. 2). Obviously, fast quasifission is negligible in these S-induced reactions, which is consistent with expectations from a systematic analysis of the presence of fast quasifission [17].

The observed significantly higher fusion hindrance for $^{34}S + ^{208}Pb$ compared to $^{36}S + ^{206}Pb$ [25] (as shown in Fig. 1) is expected to be due to quasifission. However, the MADs of the $^{34}S + ^{208}Pb$ and $^{36}S + ^{206}Pb$ reactions do not show any significant difference. We suggest an increased probability of quasifission that occurs on a long time scale (slow quasifission) as the explanation for the suppression of ER cross sections for the $^{34}S + ^{208}Pb$ reaction. The presence of slow quasifission cannot be proven from the MADs, but neither can it be excluded. Slow quasifission (also called deep quasifission) has been discussed in Refs. [33,44–46] by combining experimental data and/or theoretical approaches. Despite being slower than fast quasifission, it is expected to occur on a faster time scale than a typical fusion-fission event, where there is usually time for one or more neutrons to be evaporated before fission occurs [47,48].

The next question we address is whether detailed comparison of the mass distribution spectra for the S + Pb reactions and the $^{12}C + ^{235}U$ reference reaction can provide information on the presence and characteristics of long-time-scale quasifission for the different S + Pb reactions.

B. Fission mass distributions

The unmirrored mass spectra (presented in Fig. 2) do not in general show a pure Gaussian shape, usually having a distinctly flat-topped shape. This complicates the comparison of experimental data, because the spectra cannot be fully characterized by a single parameter (e.g., Gaussian width). Because no correlation of mass with angle was observed in the experiments, and the spectra in Fig. 2 show no systematic asymmetry about $M_R = 0.5$, any deviation from a Gaussian form should be identical on either side of the symmetric mass-split. For this reason, the mass spectra have been mirrored (averaged on either side of the line of symmetric mass-splits) and are shown in Fig. 3 for $^{12}C + ^{235}U$ and each of the S + Pb reactions, as a function of the excitation energy E^*. The best-fitting Gaussians are shown by smooth lines, which make the deviations from a Gaussian shape very clear.

1. *Analysis of mass widths*

Because the mass distributions deviate from a Gaussian shape, we have first chosen to evaluate the mean square deviation (σ^2_{RMS}) from the average ($M_R = 0.5$) for each measured mass distribution to provide a quantitative measure of the mass width. These values are plotted in Fig. 4(a) for the four reactions as a function of E^*. We see that overall the mass distributions are broader for the S + Pb reactions than for the $^{12}C + ^{235}U$ reaction at the same E^*. The widths for the three S + Pb reactions are not very different. Because of the non-Gaussian nature of the mass spectra, the detailed dependence of the variance of the mass distributions as a function of reaction and bombarding energy may well have a complex behavior. A number of physical effects can be expected to affect the width and shape of the distributions. If the mass-asymmetric component is attributed to quantum shell effects, then as the temperature increases, this contribution to the width should become attenuated, decreasing the variance. However, the thermal fluctuations will increase with temperature, which will counteract this decrease. The effect of increasing angular momentum with increasing bombarding energy should also be taken into account. However, how this affects the mass-asymmetric

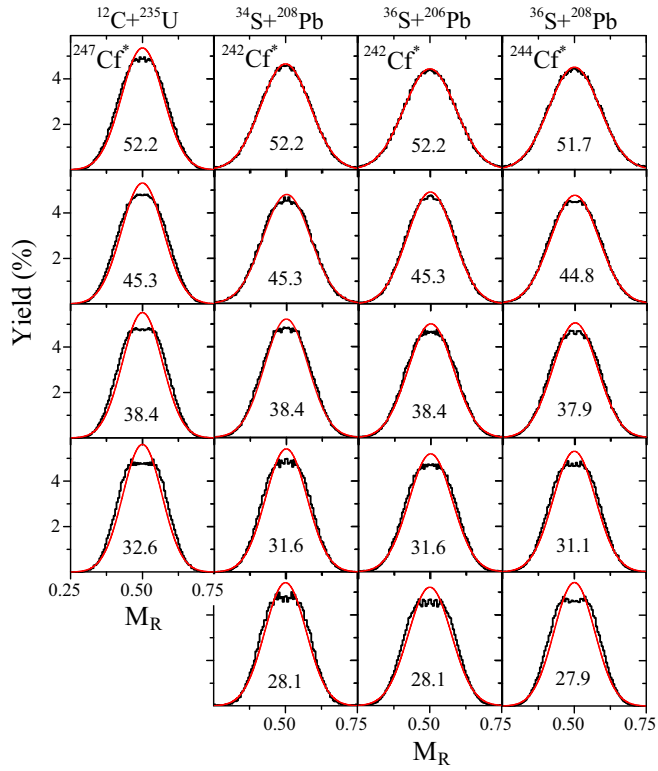

FIG. 3. (Color online) Experimental M_R distributions of fission fragments originating from the $^{12}C + ^{235}U$, $^{36}S + ^{208}Pb$, $^{36}S + ^{206}Pb$, and $^{34}S + ^{208}Pb$ reactions leading to $^{247}Cf^*$, $^{244}Cf^*$, and $^{242}Cf^*$ are shown by histograms. Excitation energies of the corresponding CN are given. The smooth lines in red show best-fitting Gaussian functions.

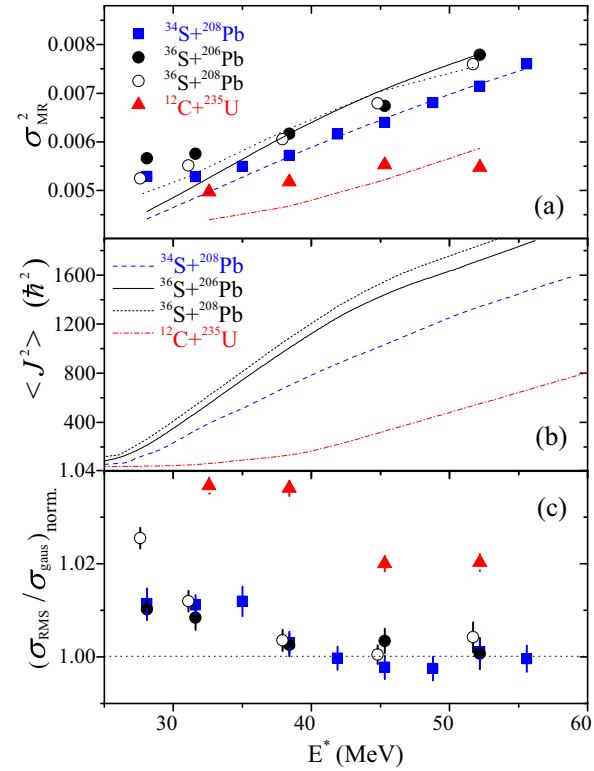

FIG. 4. (Color online) Experimental (symbols) and calculated (lines) mean square deviations (a), mean squared angular momenta (b), and $(\sigma_{RMS}/\sigma_{gaus})_{norm.}$ (c) values. The dotted line in panel (c) indicates the value 1 for the ratio.

component is not well known. If quasifission is present, it might be expected that the probability will increase with angular momentum, but this cannot be quantitatively predicted, nor can the mass width for slow quasifission. It may reasonably be expected that the quasifission component should have a mass width larger than that of the fusion-fission component.

Given that the mass widths of either component cannot yet be predicted reliably, we have used a general relationship [14,30,49] to fit the measured fission mass widths. A dependence of the variance on temperature T and mean square angular momentum $\langle J^2 \rangle$ is related through two empirical coefficients, C_T and C_J:

$$\sigma^2_{MR} = C_T T + C_J \langle J^2 \rangle. \quad (2)$$

To apply this equation, the temperature was calculated at the saddle point using the relation

$$T = [(E^* - B_f(J) - E_{rot}(J) - (\nu_{pre} 10\,\text{MeV})/a]^{1/2}, \quad (3)$$

where B_f and E_{rot} are the fission barrier and the rotational energy of the excited CN with angular momentum J and were taken from rotating liquid drop model (RLDM) calculations [50]. The number of prefission neutrons ν_{pre} was estimated using the empirical expression given in Ref. [14]. The level density parameter, a, was taken to be $A_{CN}/10\ \text{MeV}^{-1}$.

The mean square angular momentum as a function of energy was calculated for each reaction using the coupled-channels code CCFULL [51]. Taking into account the couplings of low-lying excited states [25,52,53] and deformations as appropriate, the experimental capture cross sections were reproduced where known.

The $\langle J^2 \rangle$ values are shown in Fig. 4(b). The larger angular momentum for the S-induced reactions compared with the $^{12}C + ^{235}U$ reaction at the same E^* does correlate with the mass variances observed. To attempt to quantify the relationship, we have determined the coefficients C_T and C_J for the $^{34}S + ^{208}Pb$ reaction, for $E^* > 35$ MeV, for which the data are the most extensive. The extracted values of $C_T = 4.54(16)10^{-3}\ \text{MeV}^{-1}$ and $C_J = 1.91(14)10^{-6}\ \hbar^{-2}$ were then used to make predictions for all reactions. These are shown in Fig. 4(a). Although the calculations reproduce well the limited range of data that were fitted, they fail at low excitation energies and for the $^{12}C + ^{235}U$ reaction. In view of the complexity of the situation described above, it is hard to know how to interpret this comparison or the values of the empirical coefficients C_T and C_J, except that the changes in the measured variance between the different S + Pb reactions are very small, and the increase from the results for the $^{12}C + ^{235}U$ reaction is also quite small. Thus the characteristics of the slow quasifission mass distributions appear similar to those from fusion-fission.

2. *Energy dependence of the shape of the mass distributions*

The deviation of the mass distributions from a Gaussian shape has been quantified in this work by evaluating the

ratio between the RMS deviation and the width of the best-fitting Gaussian ($\sigma_{\rm gaus}$). To ensure no bias, this ratio was normalized to the equivalent ratio built from randomly generated Gaussian events with a width of $\sigma_{\rm gaus}$. This was done to exclude an artificial reduction of RMS values within the experimentally accessible range of $M_R = 0.25$–0.75, which cuts the extreme tails of the distributions. The normalized variable $(\sigma_{\rm RMS}/\sigma_{\rm gaus})_{\rm norm.}$ can then be used for a quantitative representation of the agreement between the experimental and the Gaussian shapes. A good description of the experimental M_R distribution by a single Gaussian implies $(\sigma_{\rm RMS}/\sigma_{\rm gaus})_{\rm norm.} \approx 1$. The obtained $(\sigma_{\rm RMS}/\sigma_{\rm gaus})_{\rm norm.}$ values are shown in Fig. 4(c) as a function of E^*.

For the S-induced reactions, $(\sigma_{\rm RMS}/\sigma_{\rm gaus})_{\rm norm.}$ are equal to 1 within error bars at $E^* > 40$ MeV [see Fig. 4 (c)]. This indicates that the M_R distributions are well described by a single Gaussian and are thus consistent with the RLDM, which predicts a symmetric-peaked fission mass-split. However, at lower E^*, $(\sigma_{\rm RMS}/\sigma_{\rm gaus})_{\rm norm.}$ values differ from 1, which demonstrate that the M_R distributions are not describable by single Gaussians (as seen in Figs. 3 and 4). The deviations for the three S + Pb reactions are very similar. Large deviations of $(\sigma_{\rm RMS}/\sigma_{\rm gaus})_{\rm norm.}$ from the value of 1 were found for ^{12}C + ^{235}U at all measured E^*, consistent with visual inspection of Figs. 3 and 4.

3. *Role of sequential neutron emission*

The flat-topped mass distributions signal the importance of shell effects in the fission mass spectra. In this mass region shell effects are expected to wash out quite quickly with increasing excitation energy. Thus the excitation energy at which fission occurs is important, and multichance fission must be considered as discussed below.

The competition between neutron evaporation and fission determines multichance fission distributions and the survival probability of xn ER. This competition is quantified through the ratio Γ_n/Γ_f, where Γ_n and Γ_f are the widths for neutron evaporation and fission, respectively [6,7], at a given excitation energy. Accurate theoretical estimation of these quantities for heavy CN is complicated due to both the scarcely known height of the fission barrier and the level density of the CN [7,14,20–22]. The fission barrier of the excited CN is often presented as the sum of the liquid drop and shell correction terms. With increasing E^* the shell effects wash out, and the barrier becomes smaller, thereby lowering the survivability of the CN through the evaporation of neutrons. Therefore, for a long time it was believed that forming a CN at the lowest E^* possible would result in the highest survival probability.

Indeed, superheavy elements with Z up to 113 have been synthesized in so-called cold fusion reactions leading to low CN E^* of about 15 MeV resulting in formation of ER by the evaporation of a single neutron [1,4]. However, surprisingly, superheavy elements with $Z = 108$ and 112–118 have been synthesized in ^{48}Ca-induced fusion reactions with actinide targets at CN E^* of about 40 MeV with non-negligible survival probabilities [2,3]. Furthermore, sequential evaporation of three to eight neutrons from Cf CN produced in ^{12}C + $^{233-236,238}$U reactions at E^* up to 80 MeV is experimentally known from ER excitation function measurements [54,55]. Maxima of ER excitation functions for all three S-induced reactions (^{34}S + ^{208}Pb, ^{36}S + ^{206}Pb [25,36], and ^{36}S + ^{208}Pb [56]) and for ^{12}C + ^{235}U [54] have been observed at CN E^* of 20–40 MeV (see Fig. 1) and 32–55 MeV, respectively, where flat-topped mass distributions were observed in this work. These provide experimental support for the sequential neutron evaporation from the CN leading to multichance fission that has been accepted to exist for a long time. Recently, it has been experimentally demonstrated that Γ_n is dominant over Γ_f in the first chance fission of ^{274}Hs produced in the ^{26}Mg + ^{248}Cm reaction at $E^* = 63$ MeV [57].

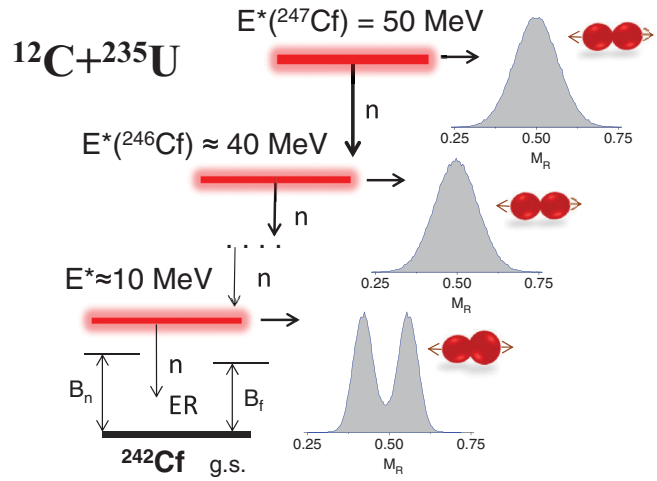

FIG. 5. (Color online) Schematic representation of multichance fission in ^{247}Cf*. Mass distributions calculated using the the general fission model code GEF are shown in gray (see text).

4. *Multichance fission*

Multichance fission following formation of the ^{247}Cf* CN produced at $E^* = 50$ MeV in a heavy-ion fusion reaction is illustrated schematically in Fig. 5. The experimental observations discussed above point to non-negligible neutron emission probabilities at high excitation energy even for such heavy CN.

That fraction of the CN which survive first chance fission will populate the daughter product ^{246}Cf* at an excitation energy reduced by the neutron binding $B_n(^{247}\text{Cf})$ and kinetic $K_n(^{247}\text{Cf}^*)$ energies of the emitted neutron. A fraction of these secondary CN again will survive against (second chance) fission. Such a cascade process will continue, leading to a population with excitation energies comparable to the neutron binding energy and fission barrier.

Finally last-chance fission may occur, at around $E^* \approx 10$ MeV, this energy being based on both the neutron binding energy and the fission barrier in neutron-deficient Cf isotopes, which are below 9 MeV [39,58]. If, instead of fission, a further final neutron evaporation occurs, this results in the formation of an ER [$W_{\rm CN}$ in Eq. (1)].

Thus, the mass distribution of fission fragments originating from the primary ^{247}Cf* CN produced at $E^* = 50$ MeV should contain fission fragments originating from different $^{247-\nu}$Cf*

nuclei excited at different $E^* = 50\ \text{MeV} - \sum[B_n(^{247-\nu}\text{Cf}) + K_n(^{247-\nu}\text{Cf}^*)]$, where ν varies from zero to the maximum possible number of chances of fission. The distribution of CN E^* from which fission occurs can be characterized by its mean, referred to henceforth as the mean excitation energy for fission.

5. Multichance fission mass distributions

As discussed in the preceding section, the cumulative mass distribution of fission fragments produced in the de-excitation cascades of highly excited CN contains the different mass distributions originating from multichance fission. Presently, the most reliable predictions of the mass distribution from excited nuclei in this mass region should be obtainable from the semiempirical GEF code [59]. The GEF code has mostly been adjusted to describe the spontaneous and light-particle-induced fission of heavy nuclei. The results of the GEF code for the mass distribution of fission fragments originating from first-, second-,..., and last-chance fission are shown in Fig. 5 by the gray shaded distributions. The mass distributions of the fission fragments originating from early chances of fission are peaked at mass symmetry, in accordance with expectations from the RLDM. The asymmetric mass distribution for low-energy fission arises because at low E^* the fission path is strongly affected by shell structures of the decaying nucleus and nascent fragments. Fission of a particular nucleus may exhibit complicated shapes of the mass distribution in low-energy fission, through the superposition of different fission pathways (modes) populating different symmetric and asymmetric mass-splits [58,60,61].

To test the predictive power of the GEF code for fission at low and high E^*, the mass distributions for fission of neutron-deficient Cf nuclei have been calculated and compared with experimental data in Fig. 6. The experimental mass distributions of low-energy fissions of ^{242}Cf* and ^{244}Cf* have been reported in Refs. [62,63] by populating them via electron capture decay of ^{242}Es and ^{244}Es, respectively. The maximum value for E^* populated in both Cf nuclei can be estimated to be 5.6 MeV taking only mass considerations into account [39]. These experimental data are well described by mass distributions calculated with GEF for neutron-induced fission, in this case calculated at $E^* = 10$ MeV.

For completeness, the high excitation energy GEF calculations (corresponding to the RLDM) were compared with mass distributions for the S-induced reactions, for which the shape could be fitted well by a single Gaussian. An example is shown in Fig. 6(c) for the mass distribution of ^{242}Cf* produced in the ^{34}S + ^{208}Pb reaction at 52.2 MeV. No evidence of shell effects is seen in the calculation, but it is somewhat narrower than that measured. For this reason, the high E^* GEF calculations were not used in fitting the current data.

We now attempt to quantitatively reproduce the flat-topped mass distributions of the current data using a triple Gaussian fit. The centers of the two Gaussians (corresponding to the mass distribution from low-energy fission) were taken from GEF calculations performed in each case for the evaporation residue preceding the final neutron evaporation step. The Gaussian widths were kept fixed at $\sigma_{\text{MR}} = 0.03$. This value was extracted

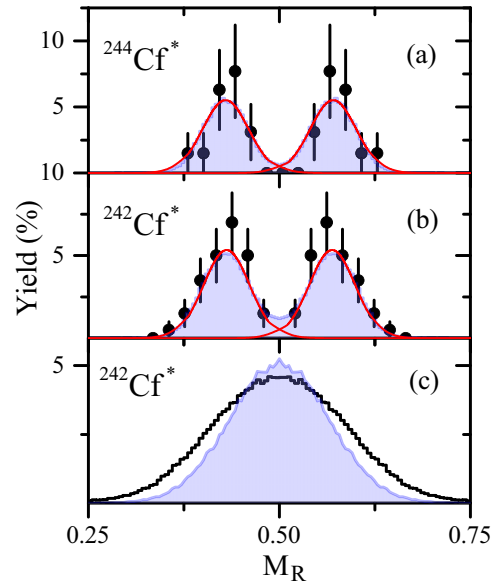

FIG. 6. (Color online) (a) Mass distribution of fission fragments of ^{244}Cf* [63] and (b) ^{242}Cf* [62] following electron capture decay of ^{244}Es and ^{242}Es (see text) and of ^{242}Cf* produced via ^{34}S + ^{208}Pb at $E^* = 52.2$ MeV (c). (a, b) Experimental data are marked by circles; blue shaded distributions correspond to results of GEF calculations (see text) at 10 MeV. Gaussian fits with $\sigma_{\text{MR}} = 0.03$ are shown by red lines. (c) The experimental distribution (black histogram) and GEF results (blue shaded spectrum) at 52 MeV are shown.

from the Gaussian fits to the GEF results shown by red lines in Fig. 6, which reproduce well the cumulative experimental mass distributions from ^{242}Cf* and ^{244}Cf*. The mass number of the nucleus undergoing fission (required for the GEF calculation) was estimated from the most probable number of evaporated neutrons, taking into account the primary excitation energies, binding [58], and mean kinetic energies (2 MeV) of each neutron. A single Gaussian with variable width, centered at $M_R = 0.5$, was used for the description of the fission component with a symmetric-peaked mass distribution. The results of the fits are presented in Fig. 7. The description of the experimental data is much better than when single Gaussian fits were used (compare Figs. 3 and 7) except for the highest energies where triple Gaussian fits were not required.

Having shown that this procedure can fit the flat-topped mass distributions, the quantitative proportions of the superposed fission components (having different mass-split characteristics) are investigated.

C. Interpretation of the mass-asymmetric fission component

The GEF calculations predict that only low-excitation-energy late-chance (mainly last-chance) fission contributes to the mass-asymmetric fission component, higher excitation energies giving symmetric-peaked Gaussian shapes. The fraction of events originating from the mass-asymmetric component ($F_{\text{asym.}}$) can be estimated from the areas of the fitted Gaussians. These fractions are given in Fig. 8 (top panel) as a function of E^*. The fraction of the mass-asymmetric component increases

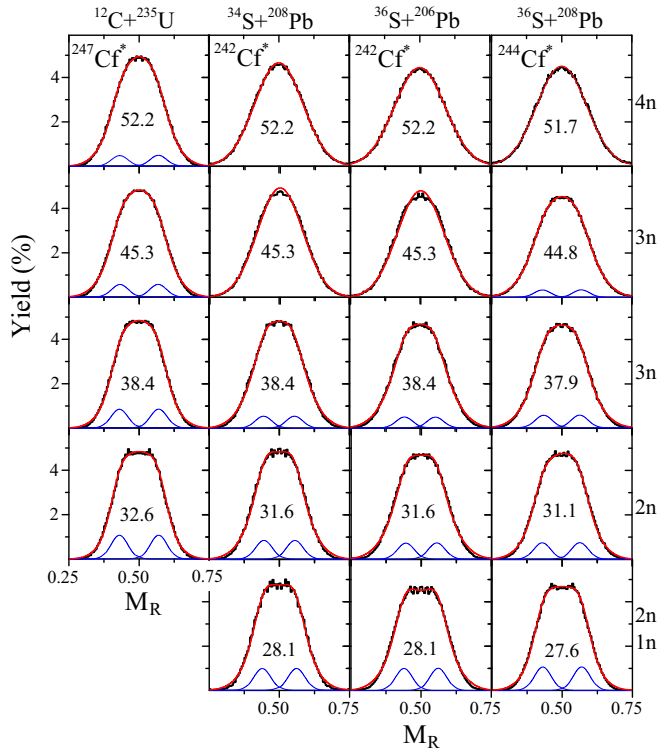

FIG. 7. (Color online) The experimental data as presented in Fig. 3, now fitted by three Gaussians. The smooth lines in red show the sum of the three Gaussian functions and the smooth lines in blue show the two Gaussians corresponding to the mass-asymmetric split. Expected numbers of neutrons emitted before formation of the ER are also shown on the right.

as E^* decreases, for all reactions. This is consistent with the fraction of late-chance fission increasing with reducing E^*, as would be expected. The fraction of the mass-asymmetric component is almost identical for the three S + Pb reactions. The more pronounced mass-asymmetric yields for ^{12}C + ^{235}U relative to ^{34,36}S at similar E^* are consistent with late-chance fission probabilities being smaller in the latter reactions. This could result from different angular momentum distributions and different quasifission probabilities.

1. *Comparison of the* S + Pb *reactions*

On the basis of this logic, the similar fractions of asymmetric fission extracted for ^{34}S + ^{208}Pb and ^{36}S + ^{206}Pb at the same E^* would be attributed to similar late-chance fission probabilities, because the reactions form the same ^{242}Cf* CN, and the capture angular momentum distributions are similar, as shown in Fig. 4(b). To explain the relationship between the fraction of asymmetric fission and the xn ER yield, a simplified expression for the fraction of asymmetric fission, $F_{\text{asym.}}$, can be written (as explained next) assuming that only last-chance fission contributes to the mass-asymmetric fission yield. For a reaction leading to "x" neutrons emitted before the xn ER is formed, let us consider the preceding nucleus after "$x-1$" neutrons have been emitted by the CN. Quantities related to this nucleus will be given the subscript $(x-1)$. Because only this nucleus is assumed to give mass-asymmetric

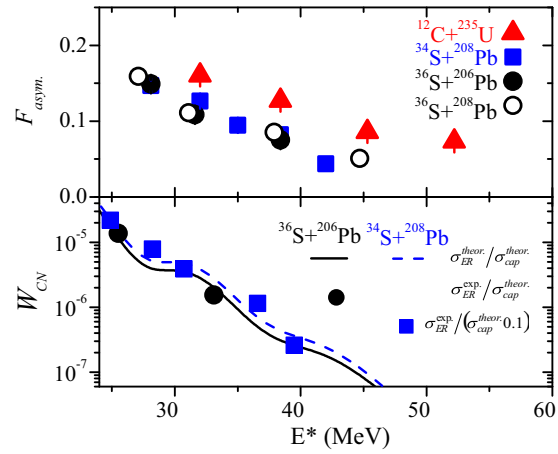

FIG. 8. (Color online) Top panel: Extracted fractions of the mass-asymmetric fission component of the M_R distributions for ^{242}Cf*, ^{244}Cf*, and ^{247}Cf*. Bottom panel: Survival probabilities, W_{CN}, of the ^{242}Cf* CN formed in ^{34}S + ^{208}Pb and ^{36}S + ^{206}Pb reactions. These values were extracted using the data shown in Fig. 1, which was taken from Refs. [25,36].

fission, the fraction of asymmetric fission in the total ($F_{\text{asym.}}$) is proportional to the total capture cross section σ_{cap} and several angular momentum averaged probabilities: that of forming (after capture) a compact CN P_{CN}, the probability $W_{(x-1)}$ of the nucleus "$x-1$" being produced (i.e., surviving previous stages of CN fission), and finally the probability $P^f_{(x-1)}$ that it undergoes fission:

$$F_{\text{asym.}} = \frac{\sigma_{\text{cap}} P_{\text{CN}} W_{(x-1)} P^f_{(x-1)}}{\sigma_f}. \tag{4}$$

Here σ_f is the total fission cross section. For these reactions, $\sigma_f \simeq \sigma_{\text{cap}}$, because the ER cross section is many orders of magnitude smaller than the total fission, allowing the following simplification:

$$F_{\text{asym.}} \simeq P_{\text{CN}} W_{(x-1)} P^f_{(x-1)}. \tag{5}$$

The probability with respect to total capture of forming an xn ER can be written in a similar way:

$$P_{xn} = P_{\text{CN}} W_{(x-1)} P^n_{(x-1)}, \tag{6}$$

where $P^n_{(x-1)}$ is complementary to $P^f_{(x-1)}$, being the probability of emitting the last neutron, leading to an xn ER, rather than undergoing fission. The last two terms in Eqs. (5) and (6) are properties of the relevant nuclei themselves and independent of the method of formation. Thus in comparing the ^{34}S + ^{208}Pb and ^{36}S + ^{206}Pb reactions, under the assumption that mass-asymmetric fission only results from last-chance fission, the very similar experimental values of $F_{\text{asym.}}$ for the two reactions require that the values of P_{CN} (and thus P_{xn}) should be similar. However, this is in conflict with the analysis of the capture and xn ER cross sections shown in Fig. 1, which indicate that the P_{CN} values differ by a factor of 10. This factor is illustrated clearly in Fig. 8(b), where W_{CN} is extracted using Eq. (1), assuming $P_{\text{CN}} = 1$ for ^{36}S + ^{206}Pb and $P_{\text{CN}} = 0.1$

for $^{34}S + ^{208}Pb$. With these assumptions the experimental data overlap.

2. Persistence of shell effects in quasifission

We propose that the discrepancy for these two reactions between the similar fractions of the mass-asymmetric fission component and the very different values of P_{CN} can be resolved by attributing a large part of the mass-asymmetric (as well as mass-symmetric) fission component to slow quasifission, rather than exclusively to last-chance (or late-chance) fission of the CN. The mass-asymmetric component must also contain a component of late-chance fusion-fission, because the finite measured ER cross sections for these two S + Pb reactions show that there must be last-chance fusion-fission. However, as argued above, the similarity of the mass spectra indicates that this fraction must be rather small.

To quantify the above discussion, we can place numbers in the above equations, using two extreme scenarios.

The first is that the average true fusion probability (P_{CN}) for $^{36}S + ^{206}Pb$ is 1, whilst that for $^{34}S + ^{208}Pb$ is $P_{CN} = 0.1$, giving a factor of 10 difference in expected ER yields as observed experimentally, as seen in Fig. 8(b). The mass-asymmetric late-chance fusion-fission contribution for the latter reaction would be only 10% of that for the former. However the current fission measurements show the mass-asymmetric components have almost identical weights. This scenario is not consistent with the fission data.

The second scenario is that P_{QF} is 0.90 (or any value close to unity, e.g., 0.99) for $^{36}S + ^{206}Pb$ and 0.99 (or, e.g., 0.999) for $^{34}S + ^{208}Pb$, giving the same factor 10 reduction in the xn ER cross section as seen experimentally for the $^{34}S + ^{208}Pb$ reaction. In this case, the contributions of late-chance fission are so small that their difference will make a negligible difference to the total mass distribution. This is consistent with the measurements. However, the considerable fraction of mass-asymmetric fission observed experimentally must in this scenario be attributed largely to quasifission. This means that shell effects must still affect the quasifission dynamics and thus mass distributions in these reactions up to equivalent CN excitation energies of ≈ 45 MeV. This is inconsistent with the excitation energy dependence of the washing out of shell effects in the GEF calculations. If shell effects persisted to higher excitation energies than predicted by GEF, they might well affect fusion-fission mass distributions at similar excitation energies. This suggestion needs further experimental investigation.

Shell effects might also be expected to affect the fast quasifission mass spectrum measured for $^{44}Ca + ^{198}Pt$ at similar E^*. Indeed, where there are flat-topped distributions for the S-induced reactions, the $^{44}Ca + ^{198}Pt$ mass spectra (see Fig. 2) also seem to show a consistent feature. Of course due to the different path in deformation space for this reaction, the detailed effects of shell structure may differ. Nevertheless, the experimental data are all consistent with the hypothesis that shell effects are still playing a role in determining the mass distribution up to $E^* \approx 45$ MeV.

The strongly hindered ER yield for the $^{34}S + ^{208}Pb$ reaction compared with the $^{36}S + ^{206}Pb$ reaction indicates that the quasifission competition is weaker in the $^{36}S + ^{206}Pb$ reaction. This must be attributed to the different nuclear structures of the reaction partners in the two reactions and the closer matching of N/Z ratios in the latter reaction, as found in Ca + Pb reactions [37]. Through a reduced rate of energy dissipation [37], this could lead to the formation of more compact composite systems inside the unconditional fission saddle point.

As argued above, the characteristics of the fission mass and angle spectra for the S + Pb reactions suggest that the quasifission component occurs on a time scale that is slow compared to the rotation time ($\sim 10^{-20}$ s) and that the probability is large in both reactions. It appears that the difference in dynamics is only visible in the tail of the probability distribution, namely, that part which results in true fusion and ER formation. This seems to be a reasonable picture and consistent with a recent systematic study of quasifission signatures [35].

IV. SUMMARY AND CONCLUSION

The present work was motivated by the previously reported measurements of evaporation residue and capture cross sections for the reactions of $^{34}S + ^{208}Pb$ and $^{36}S + ^{206}Pb$, both forming the compound nucleus ^{242}Cf. The $^{34}S + ^{208}Pb$ xn evaporation residue cross sections were 10 times smaller than expected based on the $^{36}S + ^{206}Pb$ yields, assuming both reactions proceed by fusion followed by compound nucleus fission. The difference could be explained by a smaller quasifission probability, and a consequently larger probability of forming a compact compound nucleus, in the $^{36}S + ^{206}Pb$ reaction.

To understand the difference between these two reactions, an extensive series of fission measurements has been carried out for these reactions. Measurements have also been made for the reference reactions $^{12}C + ^{235}U$ and $^{44}Ca + ^{198}Pt$ and for $^{36}S + ^{208}Pb$.

Mass and mass-angle distributions have been measured at beam energies corresponding to excitation energies of the compound nucleus in the range of 27–56 MeV. A correlation of the mass and the angle of the fission fragments was observed for the $^{44}Ca + ^{198}Pt$ reaction, indicating the presence of fast quasifission as expected. The S + Pb reactions, as well as the $^{12}C + ^{235}U$ reaction, showed no correlation of mass with angle. Thus the quasifission in the S + Pb reactions must have a time scale ($> 10^{-20}$s) considerably longer than that seen in the $^{44}Ca + ^{198}Pt$ reaction.

Flat-topped (non-Gaussian) fission mass distributions were observed for $^{12}C + ^{235}U$ at all measured E^* of the compound nucleus. This is attributed to shell effects, expected to be most prominent at low E^*. Similar but less pronounced flat-topped distributions were also observed for all three S-induced reactions at $E^* < 45$ MeV. This could, in principle, be attributed to late-chance fission and/or shell effects in the quasifission dynamics and thus mass distributions.

A 10 times suppression of experimental evaporation residue yields measured for the $^{34}S + ^{208}Pb$ reaction compared to those calculated which describe the experimental evaporation residue data for $^{36}S + ^{206}Pb$ suggests that late-chance fission should differ by a similar factor. Assuming the mass-asymmetric fission was from late-chance fusion-fission, this should give very different contributions from

mass-asymmetric fission for the two reactions. However, there was little measurable difference between the mass distributions and the deduced fraction of mass-asymmetric fission from these reactions at the same E^*. Thus the mass-asymmetric component in the S-induced reactions should not arise mainly from late-chance fission.

As argued in Sec. III C, these facts, when combined, suggest to us the following conclusions.

(i) The probability of slow quasifission is large for the $^{36}S + ^{206}Pb$ reaction and larger still for the $^{34}S + ^{208}Pb$ reaction.

(ii) Shell effects are manifested in the slow quasifission mass distributions up to equivalent compound nucleus excitation energies of ≈ 45 MeV.

(iii) The evaporation residue excitation functions for both $^{36}S + ^{206}Pb$ and $^{34}S + ^{208}Pb$ reactions should be re-measured over a wider range of excitation energies to confirm the magnitude of the larger fusion inhibition for the latter reaction.

These results should stimulate future measurements of *both* fission fragments and evaporation residues in reactions forming heavy elements to understand fully the effects and properties of the slow quasifission that appears to be very important in these S + Pb reactions.

A broader message is that studies of fusion reactions like these can reveal evidence of previously unobserved phenomena. These arise from the complicated dynamical evolution of the dinuclear system. The development of parameter-free dynamical approaches to modeling heavy ion reactions is therefore desirable for a full predictive capability of how best to produce heavy and superheavy elements and their isotopes.

ACKNOWLEDGMENTS

We are indebted to Dr. N. Lobanov and the staff of the ANU Heavy Ion Accelerator Facility for their assistance with accelerator operations. J.K. thanks the Australian National University for financial support during his stay at the ANU. The authors are grateful for fruitful discussions with Professor Dr. S. Hofmann, Dr. K. Nishio, and Dr. C. Simenel. This work was supported by Australian Research Council Grants DP110102858, FL110100098, DP130101569, and DP140101337.

[1] S. Hofmann and G. Münzenberg, Rev. Mod. Phys. **72**, 733 (2000).
[2] Yu. Ts. Oganessian, J. Phys. G: Nucl. Part. Phys. **34**, R165 (2008).
[3] Yu. Ts. Oganessian *et al.*, Phys. Rev. Lett. **104**, 142502 (2010).
[4] K. Morita *et al.*, J. Phys. Soc. Jpn. **81**, 103201 (2012).
[5] J. Khuyagbaatar *et al.*, Scientific Report 2012. GSI Helmholtzzentrum für Schwerionenforschung, Darmstadt, Germany, Report 2013-1, Darmstadt, Germany (2013), p. 131.
[6] R. Vandenbosch and J. R. Huizenga, *Nuclear Fission* (Academic, New York, 1973).
[7] R. Bass, *Nuclear Reactions with Heavy Ions* (Springer-Verlag, Berlin, 1980).
[8] W. J. Swiatecki, Phys. Scr. **24**, 113 (1981).
[9] R. Bock *et al.*, Nucl. Phys. A **388**, 334 (1982).
[10] B. B. Back, R. R. Betts, K. Cassidy, B. G. Glagola, J. E. Gindler, L. E. Glendenin, and B. D. Wilkins, Phys. Rev. Lett. **50**, 818 (1983).
[11] B. B. Back *et al.*, Phys. Rev. C **32**, 195 (1985).
[12] J. Toke *et al.*, Nucl. Phys. A **440**, 327 (1985).
[13] W. Q. Shen *et al.*, Phys. Rev. C **36**, 115 (1987).
[14] M. G. Itkis and A. Ya. Rusanov, Phys. Part. Nucl. **29**, 160 (1998).
[15] D. J. Hinde, M. Dasgupta, and A. Mukherjee, Phys. Rev. Lett. **89**, 282701 (2002).
[16] M. G. Itkis *et al.*, Nucl. Phys. A **787**, 150 (2007).
[17] R. du Rietz *et al.*, Phys. Rev. C **88**, 054618 (2013).
[18] M. G. Itkis *et al.*, Nucl. Phys. A **834**, 374 (2010).
[19] B. B. Back *et al.*, Rep. Mod. Phys. **86**, 317 (2014).
[20] W. Reisdorf, Z. Phys. A **300**, 227 (1981).
[21] G. G. Adamian, N. V. Antonenko, and W. Scheid, Phys. Rev. C **69**, 044601 (2004).
[22] V. I. Zagrebaev, Y. Aritomo, M. G. Itkis, Y. T. Oganessian, and M. Ohta, Phys. Rev. C **65**, 014607 (2001).
[23] R. Yanez, W. Loveland, J. S. Barrett, L. Yao, B. B. Back, S. Zhu, and T. L. Khoo, Phys. Rev. C **88**, 014606 (2013).
[24] A. C. Berriman *et al.*, Nature (London) **413**, 144 (2001).
[25] J. Khuyagbaatar *et al.*, Phys. Rev. C **86**, 064602 (2012).
[26] D. J. Hinde *et al.*, Phys. Rev. Lett. **74**, 1295 (1995).
[27] D. J. Hinde *et al.*, Nucl. Phys. **592**, 271 (1995).
[28] J. C. Mein, D. J. Hinde, M. Dasgupta, J. R. Leigh, J. O. Newton, and H. Timmers, Phys. Rev. C **55**, R995 (1997).
[29] A. Yu. Chizhov *et al.*, Phys. Rev. C **67**, 011603(R) (2003).
[30] G. N. Knyazheva *et al.*, Phys. Rev. C **75**, 064602 (2007).
[31] R. Rafiei *et al.*, Phys. Rev. C **77**, 024606 (2008).
[32] R. G. Thomas *et al.*, Phys. Rev. C **77**, 034610 (2008).
[33] K. Nishio *et al.*, Phys. Rev. C **82**, 024611 (2010).
[34] K. Nishio *et al.*, Phys. Rev. C **82**, 044604 (2010).
[35] E. Williams *et al.*, Phys. Rev. C **88**, 034611 (2013).
[36] J. Khuyagbaatar *et al.*, Eur. Phys. J. A **46**, 59 (2010).
[37] C. Simenel *et al.*, Phys. Lett. B **710**, 607 (2012).
[38] M. B. Tsang *et al.*, Phys. Rev. C **28**, 747 (1983).
[39] M. Wang *et al.*, Chin. Phys. C **36**, 1603 (2012).
[40] R. Bass, Phys. Rev. Lett. **39**, 265 (1977).
[41] D. J. Hinde, M. Dasgupta, J. R. Leigh, J. C. Mein, C. R. Morton, J. O. Newton, and H. Timmers, Phys. Rev. C **53**, 1290 (1996).
[42] R. du Rietz *et al.*, Phys. Rev. Lett. **106**, 052701 (2011).
[43] D. J. Hinde, D. Hilscher, H. Rossner, B. Gebauer, M. Lehmann, and M. Wilpert, Phys. Rev. C **45**, 1229 (1992).
[44] M. G. Itkis, Y. T. Oganessian, and V. I. Zagrebaev, Phys. Rev. C **65**, 044602 (2002).
[45] E. M. Kozulin *et al.*, Phys. Lett. B **686**, 227 (2010).
[46] Y. Aritomo and M. Ohta, Nucl. Phys. A **753**, 152 (2005).
[47] D. J. Hinde *et al.*, Nucl. Phys. A **452**, 550 (1986).
[48] D. J. Hinde *et al.*, Phys. Rev. C **39**, 2268 (1989).
[49] C. Lebrun *et al.*, Nucl. Phys. A **321**, 207 (1979).

[50] A. J. Sierk, Phys. Rev. C **33**, 2039 (1986).
[51] K. Hagino *et al.*, Comput. Phys. Commun. **123**, 143 (1999).
[52] S. Raman *et al.*, At. Data Nucl. Data Tables **36**, 1 (1987).
[53] R. H. Spear, At. Data Nucl. Data Tables **42**, 55 (1989).
[54] T. Sikkeland *et al.*, Phys. Rev. **169**, 1000 (1968).
[55] R. J. Silva *et al.*, Phys. Rev. C **2**, 1948 (1970).
[56] J. Khuyagbaatar (unpublished).
[57] R. Yanez *et al.*, Phys. Rev. Lett. **112**, 152702 (2014).
[58] P. Möller, A. J. Sierk, T. Ichikawa, A. Iwamoto, R. Bengtsson, H. Uhrenholt, and S. Aberg, Phys. Rev. C **79**, 064304 (2009).
[59] http://www.cenbg.in2p3.fr/GEF.
[60] P. Möller *et al.*, Nature (London) **409**, 785 (2001).
[61] Y. L. Zhao *et al.*, Phys. Rev. Lett. **82**, 3408 (1999).
[62] D. A. Shaughnessy *et al.*, Phys. Rev. C **61**, 044609 (2000).
[63] D. A. Shaughnessy *et al.*, Phys. Rev. C **65**, 024612 (2002).